Sex-dependent neural plasticity in response to damage

Marina Recatalà-Martinez[1], Manel Bosch[2], Pedro Gaspar[3], Alessandro Mineo[3], Santiago Rios[1], Irene Miguel-Aliaga[3], Marta Morey[1,4,*]

1.Departament de Genètica, Microbiologia i Estadística, Facultat de Biologia, Universitat de Barcelona, Barcelona, Spain

2. Unitat de Microscòpia Òptica Avançada, Centres Científics i Tecnològics de la Universitat de Barcelona (CCiTUB), Barcelona, Spain

3. The Francis Crick Institute, London, United Kingdom.

4. Human Genetics and Disease, Institut de Biomedicina de la Universitat de Barcelona (IBUB), Barcelona, Spain

*Corresponding author: mmorey@ub.edu

ABSTRACT

Plasticity of intact neural tissue in the vicinity of neural damage serves to restoring functionality of circuits. Much remains to be learned about the mechanisms regulating this process and the reported sex differences in recovery outcomes. Here we present the fly gut and its innervation as simplified model to address these questions. We show that gut damage caused by ingestion of toxic agents resulted in plasticity of the enteric neuronal network, manifested as a Reactive Oxygen Species (ROS)-dependent increase in neural tissue, which was reversible after a recovery period. Interestingly, males did not display neural plasticity, and masculinization of neurons in females suppressed the damage-dependent neural growth. Together, these findings position the fly gut as a system to investigate the cellular, molecular and sex-specific underpinnings of neural plasticity, with implications for therapeutic advancements in neural circuit recovery.

INTRODUCTION

Neural plasticity encompasses two crucial mechanisms for functional recovery after injury: axonal regeneration and structural plasticity of intact neural tissue. While significant research has focused on understanding and overcoming limitations to axonal

regeneration (Mahar and Cavalli, 2018; Tedeschi and Bradke, 2017), modulating the plasticity of remaining healthy neural tissue offers an alternative approach to restoring functionality (Gao et al., 2022; Petersen et al., 2022). Indeed, extensive clinical evidence demonstrates that structural plasticity of intact neural tissue plays a vital role in functional recovery and circuit rewiring after acute damage such as stroke (Cirillo et al., 2020; Murphy and Corbett, 2009; Nudo, 2003; Sampaio-Baptista et al., 2018) or multiple sclerosis episodes (Ksiazek-Winiarek et al., 2015; Prosperini et al., 2015). Interestingly, stroke recovery outcomes differ between sexes (Turtzo and McCullough, 2008; Yu et al., 2015), potentially indicating a connection to variations in neural plasticity capacity (Hyer et al., 2018; Kirby et al., 2024).

Despite these observations, insight into the cellular and molecular mechanisms regulating the plasticity capacity of adult intact neural tissue is very limited. An obstacle to advancing our understanding in this area is the intricate biological context and associated technical challenges. Specifically, the presence of healthy neural tissue in close proximity to, or even intermingled with, damaged or dying neural tissue complicates research efforts, making it difficult to isolate and study specific structural plasticity processes. We developed a simplified paradigm that focuses on the plasticity of intact neural tissue in response to non-neural tissue damage. Our approach leverages the fact that organs are innervated by the peripheral nervous system. This allows us to use the organ as a platform for inducing diverse types of damage, exposing the intact nervous system that innervates it to different noxious stimuli and analyzing the plasticity response. This approach offers several advantages: it provides a less complex environment compared to direct neural injury models; it allows for precise control over the type and extend of non-neural tissue damage; and it enables the observation of intact neural tissue responses in a physiologically relevant context.

We used *Drosophila melanogaster*'s digestive tract as a model system. Similar to mammals the fly gut is structurally and physiologically compartmentalized (Buchon et al., 2013; Lemaitre and Miguel-Aliaga, 2013; Marianes and Spradling, 2013). The epithelium contains similar cell types: intestinal stem cells (ISCs), enteroblast progenitors (EBs) that differentiate into absorptive enterocytes (ECs) and progenitors that

give rise to secretory enteroendocrine (EEs) cells. It is surrounded by muscle, oxygenated by a vasculature-like respiratory tracheal system and innervated by neurons located in the central nervous system, the corpora cardiaca (neurosecretory structure), and the hypocerebral ganglion (HCG, one of the stomatogastric ganglia) (Kuraishi et al., 2015; Miguel-Aliaga et al., 2018). While most neurites terminate on the visceral muscles, some appear to reach the underlying epithelium (Cognigni et al., 2011; Cui et al., 2024; Kenmoku et al., 2016; Petsakou et al., 2023). Contrary to the extensive innervation along the length of the tract in mammals, innervation in the fly gut is still complex but restricted to specific regions facilitating its analysis (Kuraishi et al., 2015; Miguel-Aliaga et al., 2018). Recent studies in mammals and flies show the effects of microbiota, nutrient, sex, ageing, reproductive stage, and recovery after injury on the morphology and/or function of gastrointestinal innervation, showcasing its plasticity capacity (Ameku et al., 2020; Hadjieconomou et al., 2020; Petsakou et al., 2023). Here we analyzed the structural plasticity capacity of intact neural tissue innervating the anterior midgut in response to damage.

RESULTS

Intestinal damage induces reversible neural plasticity.

In order to quantify and characterize the innervation in the anterior part of the midgut we proceeded to select a neural driver and reporter that would specifically label neuronal processes with native GFP fluorescence. This prevented background signal from secondary antibodies and provided a high signal to noise ratio which facilitated faithful neural process quantification as GFP signal. General neuronal markers, such as Elav (Chen et al., 2016; Holsopple et al., 2022; Titos et al., 2023) or n-Synaptobrevin (Weaver et al., 2020), also label EEs. However, we used the *GMR51F12-GAL4* driver line from the Janelia FlyLight collection (Jenett et al., 2012; Min et al., 2021; Olds and Xu, 2014) and a specific *nSyb.S-GAL4* driver (Weaver et al., 2020), neither of which labels EEs. Morphological landmarks in whole-mount preparations, combined with phalloidin co-staining to visualize the surrounding musculature, enabled consistent imaging of the same digestive tract region and its associated neural innervation (Figure 1A). Using 3D reconstruction and image analysis we obtained volume quantifications for both the digestive tube and neural tissue (see Material and Methods). Scaling growth is a prevalent

97 phenomenon in the peripheral nervous system where sensory and motor neurons must
98 adjust the size of their arborizations according to the area of their target tissues to
99 maintain their functionality (Bentley and Toroian-Raymond, 1981; Bucher and Pflüger,
100 2000; Lee and Stevens, 2007; Menon et al., 2013). Measuring the volume of the digestive
101 tube enabled us to use statistical analysis methods that accounted for and removed any
102 potential influence of digestive tube size variation in adults (driven by treatment or
103 genetic background) on neural tissue quantification comparisons (see Material and
104 Methods).
105
106 To damage the gut we fed flies with DSS. DSS is a polymer that induces colitis in
107 mammals (Yang and Merlin, 2024) and has been used in *Drosophila* to study the cellular
108 mechanisms and molecular pathways that regulate ISC proliferation during regeneration
109 (Jiang et al., 2016; Tian et al., 2022). When flies ingest DSS it crosses the epithelium
110 expanding the basement membrane sheet and altering muscle morphology (Howard et
111 al., 2019). The resulting change in biomechanical forces in the niche is thought to activate
112 ISC division (Howard et al., 2019). DSS feeding also results in trachea sprouting
113 (Perochon et al., 2021), which is necessary for ISC proliferation (Perochon et al., 2021;
114 Tamamouna et al., 2021). Interestingly, basement membrane and muscle defects, as
115 well as trachea remodeling, are reversible after a recovery period (Howard et al., 2019;
116 Perochon et al., 2021; Tamamouna et al., 2021). We wondered whether adult neurons
117 were plastic and could also respond to gut damage.
118
119 To analyze the effect of gut damage on neural plasticity we fed adult mated females with
120 DSS for 4 days and compared them to controls fed with the carrier (sucrose). We
121 confirmed the effectiveness of DSS by replicating previously published observations,
122 including a reduction in lifespan (Amcheslavsky et al., 2009) (data not shown) and an
123 increase in the proliferative response of ISCs in the midgut (Amcheslavsky et al., 2009)
124 (see later in Figure 2A). Over 90% of the flies that survived the feeding protocol tested
125 negative for the SMURF assay (Rera et al., 2012), indicating that in the majority of animals
126 (93,3%±SD4.5) that were dissected gut permeability was not compromised. Thus, during
127 DSS feeding, neurons were largely shielded from direct exposure to gut contents that
128 could potentially cause damage. When we dissected the DSS-fed females and compared

them to control flies we observed a significant increase in neural tissue (Figure 1B). To rule out neurogenesis as the source of the new neural tissue, we quantified the number of neural nuclei in the HCG, the primary source of neurons innervating the anterior midgut (Figure 1A). No differences were observed between control and DSS-fed animals (Figure 1C), suggesting that the increase in neural tissue was due to neural growth. This neural growth was not exclusive to DSS damage since we also observed it when feeding the flies with H_2O_2 (Figure 1D).

Tracheal terminal cells (TTCs) are known to sprout in response to DSS and H_2O_2 (Perochon et al., 2021; Tamamouna et al., 2021). Hence, we investigated their response in the anterior midgut, where we observed the increase in neural tissue. Our findings revealed that this region was poorly tracheated, with very few TTCs (Supplementary Figure 1A) and minimal branch coverage (Supplementary Figure 1B). This pattern remained unchanged in DSS-fed flies, indicating that TTCs in this area were unresponsive to gut damage (Supplementary Figure 1A, B). Furthermore, their morphology did not account for the observed extent of neural growth, which far exceeded the coverage provided by TTCs. These findings suggested that in the anterior midgut TTCs did not serve as a physical scaffold for neural tissue growth.

We next explored the stability of this neural plasticity and conducted recovery experiments (Figure 1E). To carry out comparisons within the same cohort of flies, a subset of flies was dissected after the DSS treatment and the rest after the recovery period. While DSS feeding increased the neural tissue (C versus DSS), a 4-day recovery period (DSS + Rec) reverted the amount of neural tissue to levels as those of control flies (C + Rec). Consistent with this observation, a clear reversal of neural growth was observed when comparing flies dissected after the DSS treatment (DSS) and those dissected after the recovery phase (DSS + Rec). No differences were observed between control flies (C versus C + Rec).

In summary, these experiments indicate that the intact neural tissue innervating the digestive tube is plastic and responds to damage with growth. This neural growth is reversible after a recovery period, as the gut returns to homeostasis after injury.

161 Importantly, these observations were validated with two independent neural drivers
162 (*GMR51F12-GAL4*, Figure 1 and *nSyb.S-GAL4*, Supplementary Figure 1C).
163

Figure 1

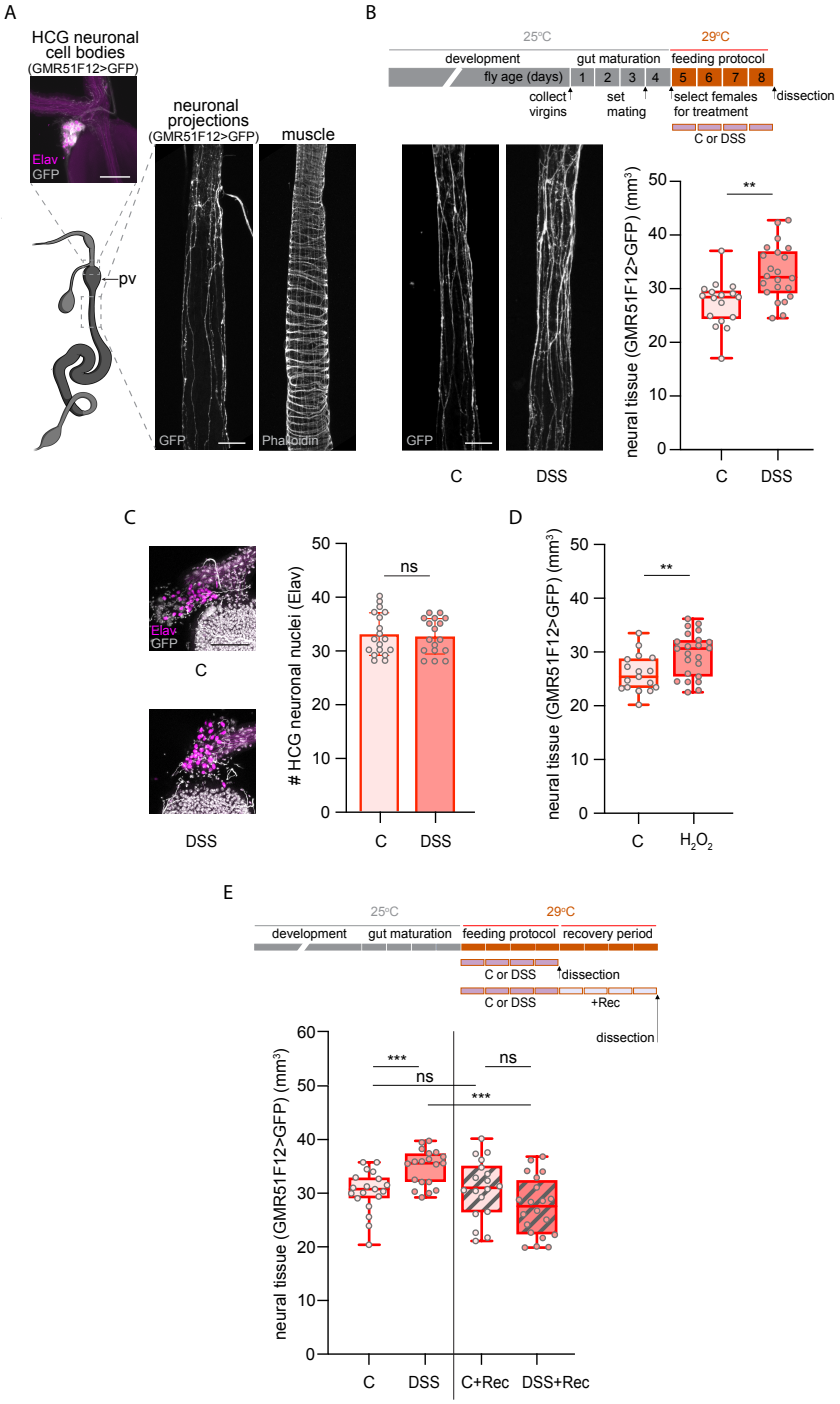

164
165

166 ***Figure 1. Neural plasticity induced by gut damage resolves after recovery.*** A) Drawing
167 of the adult gut with two areas of interest highlighted and corresponding z-stack

168 projected confocal images. The square box region corresponds to the area above the
169 proventriculus (pv) and the image shows neuronal nuclei (magenta, anti-Elav) and
170 neuronal membrane (grey, GFP) of the HCG. Autofluorescence of the peritrophic
171 membrane lining the gut in this region is observed. The rectangular box region
172 corresponds to the area of the anterior midgut imaged in subsequent analysis and the
173 images show neuronal processes (grey, GFP) and muscle fibers (grey, Phalloidin). B)
174 Schematic outlining the feeding protocol and dissection time. Z-stack projected
175 confocal images of neuronal processes innervating the anterior midgut of control (C) and
176 DSS-fed (DSS) females and quantification of neural tissue. Red outline in the box plots or
177 bar graphs indicates female. C) Z-stack projected confocal images of the HCG of control
178 and DSS-fed females stained with Hoechst (grey, which also accumulates in some
179 tracheal branches) and showing neuronal nuclei (magenta, anti-Elav). Quantification of
180 neuronal nuclei in the HCG of C and DSS-fed females. D) Quantification of neural tissue
181 in control and H_2O_2-fed females. E) Schematic outlining the feeding protocol as well as
182 the feeding protocol followed by the recovery period. Quantification of neural tissue after
183 the feeding protocol and after the recovery period (Rec). Scale bar 50μm. Statistical
184 significance is indicated as follows: * $p < 0.05$, ** $p < 0.01$, *** $p < 0.001$, n.s = not
185 significant. Gut schematic from *BioRender.com*.
186
187 **ISC proliferation does not mediate neural plasticity.**
188 Since DSS -feeding results in an increase in ISC proliferation, we set out to test if ISC cell
189 division was signaling neurons to grow. DSS-mediated ISC proliferation has been
190 described as an increase in histone 3 phosphorylation (H3P) signal along the midgut
191 (Amcheslavsky et al., 2009), mostly concentrated in its posterior part at the midgut to
192 hindgut junction. Although H3P signal in the anterior part is quite scarce if not absent in
193 control animals a significant increase in signal was detected in DSS-fed flies (Figure 2A).
194 To better monitor the extend of ISC divisions exclusively taking place during the feeding
195 protocol in the anterior part of the gut we used lineage tracing (ReDDM) (Antonello et al.,
196 2015) and observed substantial ISC proliferation in DSS-fed versus control animals
197 (Figure 2B). To test the effect of this extensive ISC proliferation on neural growth we
198 sought to block ISC cell division in adult animals at the same time they were feeding on
199 DSS to assess if neural growth would be suppressed. We blocked ISC proliferation using

200 a combination of a null allele (*Cdk1*^{null}) and a temperature-sensitive allele of *Cdk1* (*Cdk*$^{1E1-24}$) (Rodríguez et al., 2024), which rendered flies mutant for *Cdk1* during DSS feeding
202 (Figure 2C). We observed no difference in neural growth between DSS-fed flies with and
203 without proliferation blockage (Figure 2D), indicating that ISC cell division is not
204 responsible for the DSS induced neural growth.
205
206 **Gut-derived ROS stimulates neural plasticity.**
207 DSS feeding results in epithelial damage, causing cell death and an increase in ROS
208 levels (Wu et al., 2012). To test the possible contribution of ROS levels to neural growth,
209 and to overcome the limitation that using the GAL4/UAS system to visualize neurons
210 imposes on the genetic manipulation of the gut with other heterologous systems, we took
211 advantage of antioxidant drugs. To investigate if ROS could signal neurons to grow, we fed
212 flies with DSS plus the ROS inhibitor N-acetyl cysteine (NAC) and compared them to flies
213 fed with DSS only. In this case we observed a reduction of neural growth in the NAC-fed
214 condition (Figure 2E). Moreover, the neural tissue values obtained for the DSS + NAC
215 feeding protocol were not significantly different from the values observed for the Control
216 + NAC condition, arguing for a strong suppression of the neural growth (Figure 2E). Thus,
217 DSS-dependent ROS promotes neural plasticity.
218
219 **Reversal of neural growth as the gut returns to homeostasis is not caspase**
220 **dependent.**
221 We were intrigued about the mechanisms regulating the reversal of the neural growth
222 after the recovery period. Axon pruning can take place either through axon retraction or
223 degeneration (Luo and O'Leary, 2005). Examples of the latter during developmental
224 remodeling include the pruning of mushroom body gamma neurons (Watts et al., 2003)
225 as well as dendritic arborizing (da) sensory neurons ddaC (Williams and Truman, 2005).
226 While deletion of apoptotic activators or expression of a caspase inhibitor in MB neurons
227 had no effect on axon pruning (Watts et al., 2003), da neurons use local caspase
228 activation to direct dendrite engulfment (Williams et al., 2006). To test if there was a role
229 of caspases in reversal of the neural growth in the enteric nervous system, we inhibited
230 apoptosis specifically in neurons by overexpressing the caspase inhibitor Diap1. We
231 observed that reversal of neural growth still took place (Supplementary Figure 2). This

result suggests the observed reversal of neural growth could potentially be mediated by axon retraction, rather than caspase-dependent mechanisms.

Figure 2

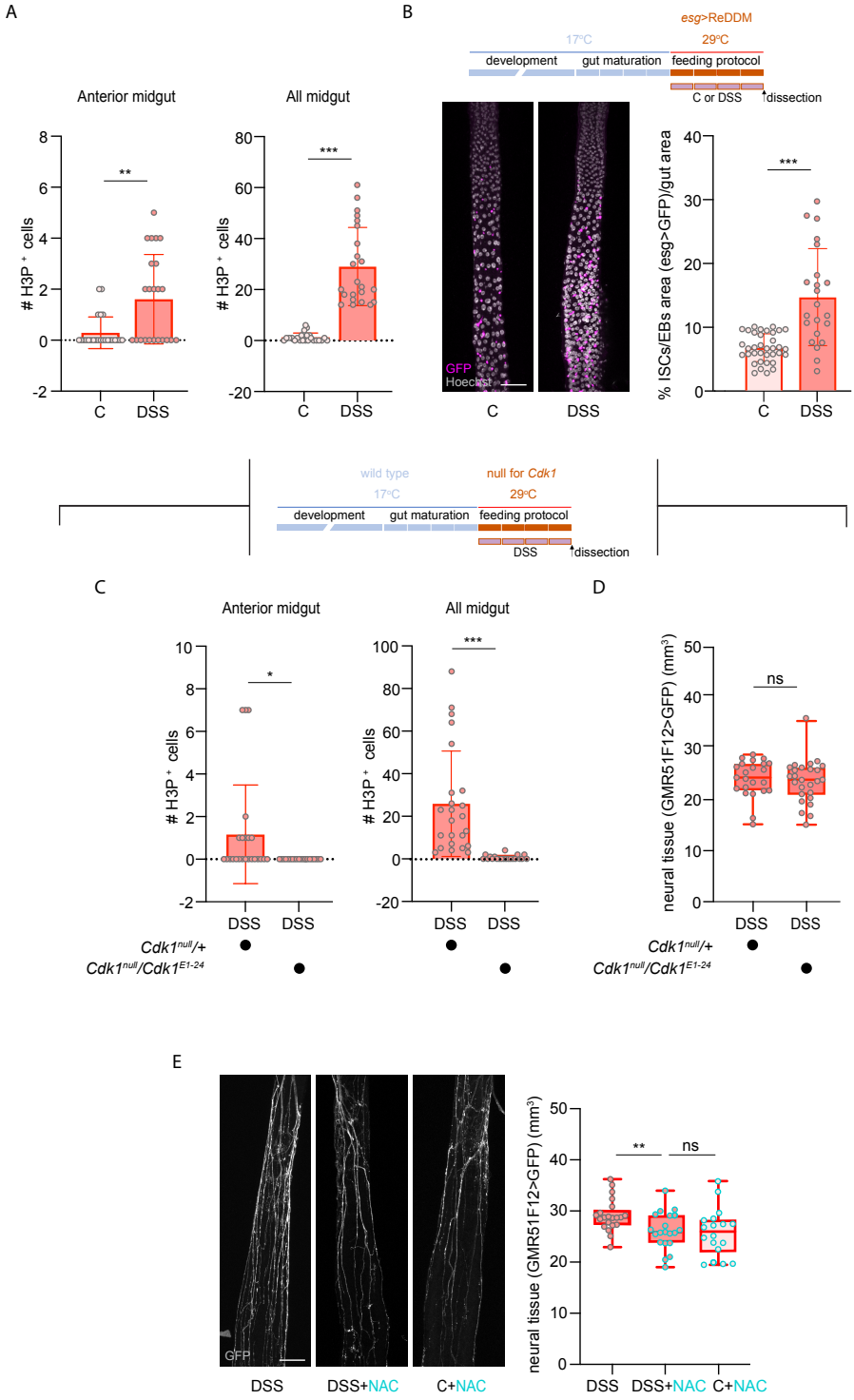

Figure 2. Neural plasticity does not depend on ISC proliferation but on gut-derived ROS. A) Quantification of H3P/Hoechst positive cells in the anterior midgut and the whole midgut in C and DSS-fed females. B) Schematic showing activation of ReDDM lineage tracing during the feeding protocol. Z-stack projected confocal images of the anterior midgut stained with Hoechst (grey) and showing the cell membrane of ISCs/EBs (magenta, anti-GFP) in C and DSS-fed females. Quantification of the percentage of the ISC/EB area (GFP signal) from the total area of the anterior mid gut in C and DSS-fed females. C-D) Schematic showing temperature dependent knock out of Cdk1 function during the feeding protocol. C) Quantification of H3P/Hoechst positive cells in the anterior midgut and the whole midgut in wild type (heterozygous) and *Cdk1* null females after DSS feeding. D) Quantification of neural tissue in wild type and *Cdk1* null females after DSS feeding. E) Z-stack projected confocal images of neuronal processes in the anterior midgut of DSS, DSS + NAC and C +NAC -fed females and quantification of neural tissue. Scale bar 50μm. Statistical significance is indicated as follows: $*\ p < 0.05$, $**\ p < 0.01$, $***\ p < 0.001$, n.s = not significant.

Neural plasticity is exclusive to females and is actively suppressed when female neurons are masculinized.

Interestingly, males did not exhibit neural growth following DSS treatment (Figure 3A). To investigate whether this neural growth was exclusive to female neurons, we aimed to create female individuals with masculinized neurons. Most sex differences in *Drosophila* arise from the female specific expression of the *Sex lethal* gene (*Sxl*) which codes for an RNA binding protein (Bell et al., 1988). Sxl induces the alternative splicing of the *transformer* (*tra*) gene generating the female fate determining TraF protein only in females (Belote et al., 1989; Boggs et al., 1987; Inoue et al., 1990; Sosnowski et al., 1989). We first confirmed that neurons in the HCG expressed the female-specific alternative splicing variant of *tra* while males didn't (Figure 3B,C) (Hérault et al., 2024). Subsequently, we proceeded to masculinize neurons in females by means of *tra* downregulation with RNAi during development (Figure 3D). We confirmed that the presence of the *UAS-Dcr2* transgene did not affect the response of wild type females to DSS, and thus, the expected increase in neural tissue was observed. Interestingly, DSS feeding did not have any effect in masculinized females and the amount of neural tissue was not significantly different

269 between control and DSS-fed flies. In addition, DSS-fed masculinized females displayed
270 significantly less neural tissue that DSS-fed control flies, aligning with the absence of
271 neural growth in masculinized females.
272

Figure 3

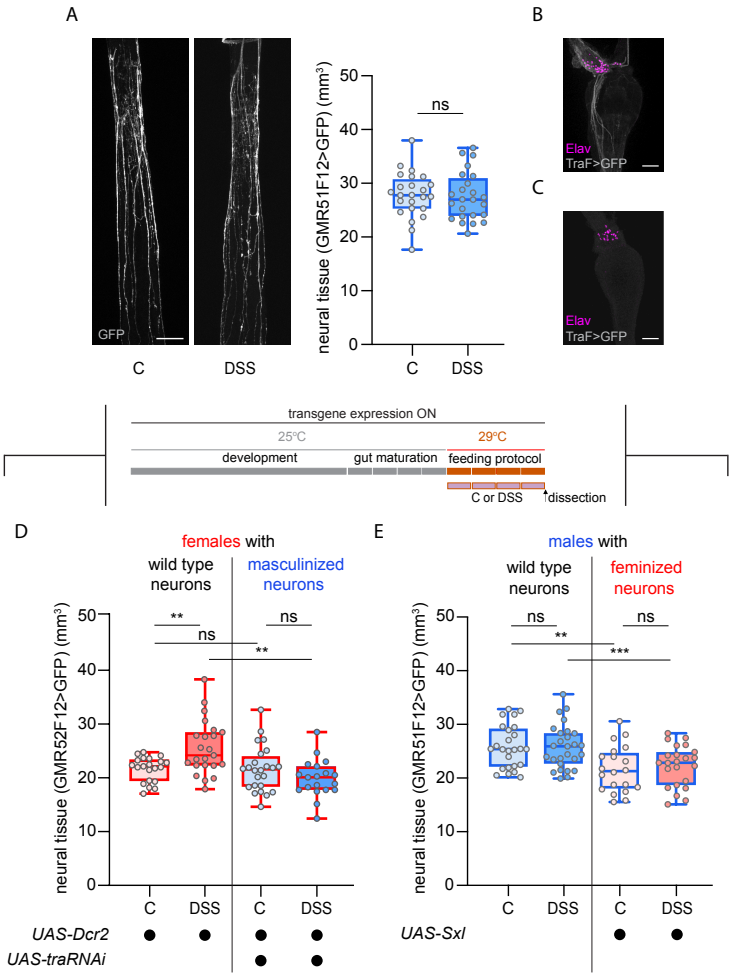

273
274

275 ***Figure 3.*** **Neural plasticity is not observed in males and masculinization of female**
276 **neurons abolishes neural growth.** A) Z-stack projected confocal images of neuronal
277 processes in the anterior midgut of C and DSS-fed males, and quantification of neural
278 tissue. Blue outline in box plots indicates male. B-C) Z-stack projected confocal images
279 at the level of the HCG showing female-specific *tra* alternative splicing in neurons (grey,
280 GFP; magenta, Elav) in females (B) and absence in males (C). D-E) Schematic showing
281 transgene expression in neurons in relation to the feeding protocol. D) Quantification and
282 comparison of neural tissue in females and females with masculinized neurons both in

283 C versus DSS-fed conditions. E) Quantification and comparison of neural tissue in males
284 and males with feminized neurons both in C versus DSS-fed conditions. Scale bar 50µm.
285 Statistical significance is indicated as follows: * $p < 0.05$, ** $p < 0.01$, *** $p < 0.001$, n.s =
286 not significant.
287
288 We also carried out the reverse experiment and attempted to confer plasticity to male
289 neurons by feminizing them through developmental *Sxl* overexpression (Figure 3E) (Bell
290 et al., 1991). In this case, the DSS treatment had no effect in feminized males, and we did
291 not observe the neural growth we expected to see for a successfully feminized male.
292 Moreover, both control and DSS-fed feminized males showed less amount of neural
293 tissue than wild type males. These results indicate that neuronal Sxl overexpression in
294 males is not sufficient to induce damage-responsive plasticity, and may even impair
295 neural tissue growth in our context.
296
297 The lack of neural growth in males following DSS-induced gut damage, along with the
298 suppression of this response in masculinized female neurons, suggests that neural
299 plasticity is limited in males compared to females.
300
301 **DISCUSSION**
302 Our findings establish the fly gut and its innervation as a tractable model to dissect the
303 mechanisms of neural plasticity in response to acute nearby tissue damage. This system
304 enables the study of both structural growth and retraction in intact adult neurons. We
305 show that DSS-induced ROS promotes neural growth, consistent with growing evidence
306 that ROS supports structural plasticity (Oswald et al., 2018). In *Drosophila*, regrowth after
307 developmental pruning and regeneration involves TOR signaling and interactions with the
308 InR/PI3K/Akt pathway (Sanal et al., 2023; Yaniv and Schuldiner, 2016). Mammals also rely
309 on mTOR for neuronal regeneration (Lund-Ricard et al., 2020). Given that low, transient
310 ROS can activate both pathways (Yoshida et al., 2011; Zhang et al., 2020), these are
311 candidates to mediate the observed DSS-dependent neural growth. Conversely, axon
312 retraction upon recovery may involve cytoskeletal remodeling via RhoA signaling. In
313 *Drosophila* there is evidence for a RhoA-mediated retraction pathway actively
314 suppressed by a GTPase-activating protein (GAP) (Billuart et al., 2001). Additionally, Rho

315 guanine nucleotide exchange factors (GEFs) have also been identified (Hakeda-Suzuki et
316 al., 2002). Thus, extracellular cues may modulate retraction via GAP/GEF balance. Given
317 its parallels with repulsive axon guidance, cell surface molecules like Ephrins, Slits, and
318 Semaphorins—which signal through RhoA (Bashaw and Klein, 2010; Kania and Klein,
319 2016; Pasterkamp, 2012)—could be expressed by the gut or muscle during recovery to
320 help coordinate neural plasticity.
321
322 In addition, we uncover a clear sexual dimorphism: neural growth is absent in males and
323 suppressed in masculinized female neurons. However, feminizing male neurons was not
324 sufficient to induce plasticity. One possibility is that signals from other feminized
325 surrounding tissues could be necessary. Indeed, sex-specific differences in morphology,
326 physiology, pathology, and cell behavior—including intestinal stem cells and
327 enterocytes—have been documented in the fly digestive system (Blackie et al., 2024;
328 Hadjieconomou et al., 2020; Hudry et al., 2019, 2016; Regan et al., 2022, 2016; Reiff et
329 al., 2015). Interestingly, although we did not detect structural changes in TTCs in the
330 anterior midgut, plasticity in the tracheal system has been reported in other regions of
331 the gut (Linneweber et al., 2014; Perochon et al., 2021; Tamamouna et al., 2021). TTC's
332 behavior is strikingly similar to that of neurons: they respond to DSS and H_2O_2 feeding
333 with ROS-dependent sprouting (Perochon et al., 2021; Tamamouna et al., 2021),
334 although sex specific differences remain to be tested. Given the recent link between the
335 dimorphic tracheal system and sex-specific gut morphology (Blackie et al., 2024), it is
336 tempting to speculate that the functional and/or structural plasticity of subsets of TTCs
337 could also be dimorphic. It is well established that sex differences influence organ
338 formation, function and physiology (Mank and Rideout, 2021). The results presented here
339 showcase the fly gut and its innervation as a model to unravel how biological sex
340 influences neural plasticity. Understanding these mechanisms could guide the
341 development of sex-specific therapeutic strategies for neural repair.
342
343 **MATERIALS AND METHODS**
344 **Fly stocks**
345 The following fly lines were used: *GMR51F12-GAL4* (BDSC:58685), *nSyb-GAL4.S* (BDSC:
346 51635), *UAS-Flybow.1.1B* (used as 10xUAS-CD8::GFP, BDSC: 56802, 56803), *DSRF.Term-*

347 *GAL4* (BDSC: 25753), *esg-GAL4* (a gift from M. Milán, unknown insertion), *UAS-*
348 *mCD8::GFP* (BDSC:5130), *UAS-H2B::RFP* (a gift from J. Morante), *tubP-GAL80*^{ts} (BDSC:
349 7017), *Cdk1*^{null} (BDSC: 6643), *Cdk*$^{1E1–24}$ (BDSC: 6641), *UAS-Diap1* (BDSC: 15310), *traF-*
350 *GAL4* (a gift from B. Hudry), *UAS-Dcr-2* (BDSC: 24650), *UAS-traRNAi.TRiPJF03132* (*UAS-*
351 *traRNAi*, BDSC: 28512), *UASp-Sxl.alt5-C8* (*UAS-Sxl*, BDSC: 58484). The list of complete
352 genotypes is available in Supplementary Information.
353
354 **Feeding protocols**
355 For feeding assays, virgin females were collected and aged on standard media at 25ºC for
356 3-4 days before undergoing mating for 24hrs. Then same procedure was carried out when
357 experiments were performed with males. Flies were recovered from the mating and
358 transferred in groups of 10 to an empty vial containing 5 pieces of 2cm × 2cm of bench
359 paper soaked with 500ml of the desired feeding solution. Flies were transferred to a new
360 vial with fresh feeding paper every day for the specified number of days prior to
361 dissection. The feeding protocol was always done at 29ºC. For DSS (Merck, 42867)
362 induced damage, flies were fed with 5% sucrose (Control) or with 6% DSS in 5% sucrose
363 (DSS) for 4 days. For the SMURF assay, the last control and DSS feeding solutions prior to
364 the day of dissection were laced with Brilliant Blue FCF (80717, Merck) at 2.5% w/v. For
365 H_2O_2 (1072100250, Merck) induced damage, flies were fed with 5% Sucrose (Control) or
366 1% H_2O_2 in 5% sucrose (H_2O_2) for 4 days. For NAC treatment, flies were fed with 1,2mM
367 NAC in 5% sucrose (Control + NAC) or 6% DSS + 1,2mM NAC in 5% sucrose (DSS + NAC)
368 for 4 days. For recovery protocols, after the DSS feeding protocol control and DSS-fed
369 flies were each transferred to vials with 5% sucrose for 4 days (Control + Recovery; DSS
370 + Recovery).
371
372 **Temperature sensitive assays**
373 To visualize the amount of proliferation taking place exclusively during the four days of
374 the feeding protocol we set ReDDM-based crosses (Antonello et al., 2015). This lineage
375 tracing approach uses the Gal80 temperature sensitive allele (*Gal80*^{ts}), which inhibits
376 GAL4 transcription at permissive temperature (19ºC) and allows it at the restrictive one
377 (29ºC) (McGuire et al., 2003), and *esg-GAL4* to label ISCs and EBs. Crosses were grown
378 and flies were kept at 17°C to ensure Gal80^{ts} repression until adult mated female flies

379 were shifted to 29°C to inactive the Gal80 and carry out the feeding protocol. To block ISC
380 proliferation during the feeding protocol, *Cdk1*^{null}/ *Cdk*$^{1E1–24}$ flies were grown, aged and
381 mated at 17°C, Cdk1 function was abrogated once the flies were transferred to 29°C
382 (Rodriguez et al., 2024) during the DSS feeding protocol.
383
384 **Dissection and immunostaining**
385 To obtain the gut flies were dissected in PBS. Adult animals had their heads cut off with
386 scissors by the neck, their abdomens were pulled apart from the thorax and opened to
387 extract the gut. With this procedure the digestive tube was severed well above the crop
388 duct. Once fat and ovaries were removed, the gut was handled by its posterior end and
389 transferred to PBS in a well drawn onto a poly-l-lysine-coated slide (P1524, Merck) using
390 hydrophobic silicone (Flowsil, Intek Adhesives). In cases were the anterior part of the
391 midgut had to be repositioned, we manipulated the gut from the crop to avoid touching
392 the digestive tube. Guts were fixed at room temperature for 30min in 4% PFA in PBS.
393 Washes were done with PBS-T (PBS, 0.25% Triton X-100). To label the muscle or nuclei,
394 guts were incubated at room temperature for 30 min with Alexa Fluor™ 635 Phalloidin
395 (1/400, A34054, Invitrogen) or Hoechst 33258 (1/1000, H3569, Invitrogen) respectively in
396 PBS-T. A final wash with PBS was done prior to mounting. When antibodies were used,
397 primaries were incubated overnight at 4°C, and secondaries were incubated at room
398 temperature for 2–3 h. The following antibodies were used: rat-anti-Elav (1/100, 7E8A10,
399 DSHB), rabbit-anti-H3P (1/1000, 06-570, EDM Milipore), rabbit-anti-DsRed (1/200,
400 632496, Clontech), chicken-anti-GFP (1/800, ab13970, Abcam), Alexa Fluor™ 568 goat-
401 anti-rat, Alexa Fluor™ 488 goat-anti-rabbit, Alexa Fluor™ 568 goat-anti-rabbit, Alexa
402 Fluor™ 488 goat-anti-chicken (1/500, A11077, A11008, A11011, A11039, Life
403 Technologies). Samples were mounted in VECTASHIELD® PLUS Antifade Mounting (H-
404 1900-10, Vector Laboratories).
405
406 **Microscopy**
407 Samples were imaged using a Zeiss LSM 880 confocal microscope (Zeiss, Germany)
408 equipped with a 25X 0.8 glycerol immersion media objective and an Argon and a
409 HeNe633 lasers. For neural network analysis, to consistently image the same region in
410 each gut, we used the end of the proventriculus as a positional landmark and captured

411 the gut section that fit within the visual field of the 25X objective at 0.8 magnification,
412 which in our set up generated images of 566,79 μm^2. As quality control for dissection,
413 only guts with an intact HCG were considered since this ganglion contains the cell bodies
414 of many of the neurons innervating the anterior midgut. Stacks of images were acquired
415 with a pixel size of 0.55x0.55x1um (xyz) and a pixel dwell time of 2.05us.
416
417 **Image processing and quantifications based on images**
418 Images were processed with Fiji (version ImageJ 1.53c, (Schindelin et al., 2012) and
419 figures assembled using Adobe Illustrator (Adobe, San Jose, CA).
420 *For quantification of neural tissue and gut parameters:* The channel with the neuron
421 staining was filtered in 3D (Ollion et al., 2013) first with the maximum filter and then with
422 the minimum one, with a radius of 3.3um in x and y and 2um in z, in both filters. Then the
423 filtered stack was processed using the Tubeness plugin (sigma = 0.66) (Sato et al., 1998).
424 Finally, images were binarized using the Bernsen's AutoLocal threshold method (radius =
425 2) (Bernsen, 1986). The resulting binary stack was analyzed first with the 3D Object
426 Counter function to obtain the total neuronal network volume (mm^3). The channel with
427 the gut staining was processed by background subtraction and then thresholder using
428 the Li's method (Li and Lee, 1993). The resulting binary stack was analyzed with the 3D
429 Object Counter function to obtain the volume of the gut.
430 *For other quantifications:* The number of Elav/Hoechst positive nuclei in the HCG was
431 counted from the confocal stack using the 3D Object Counter plugin. The number of TTC
432 nuclei was counted by hand from the confocal stack maximum projection. TTCs volume
433 was obtained using the same procedure as for neural tissue quantification. The number
434 of H3P/ Hoechst positive nuclei in the midgut was counted directly under the confocal
435 microscope. For quantification of cumulative proliferation using ReDDM, xyz stacks of
436 half the gut were taken and z-projected. The Hoechst signal was manually outlined to
437 measure the gut area. To quantify the area of GFP signal from mCD8::GFP-labeled cells
438 (representing ISCs and EBs resulting from ISCs divisions) a Gaussian Blur filter (radius =
439 2.0) was applied. The image was then thresholded using the "MaxEntropy" algorithm
440 (Kapur et al., 1985) and finally, the GFP-positive regions larger than 10μm^2 were
441 quantified. The GFP area was represented as a percentage of the total area.
442

443 **Other quantifications**

444 For the SMURF assay (Rera et al., 2012), on the 4th day of the DSS feeding protocol, we
445 assessed the proportion of surviving flies that were positive for the SMURF phenotype.

446

447 **Statistics**

448 Data analysis was carried out using Prism 6 (GraphPad Software Inc., San Diego, CA) and
449 Statgraphics Centurion version 18 (Statgraphics Technologies Inc., The Plains, VA).
450 Experiments were performed with three biological replicates yielding similar results, and
451 a representative replicate is shown. A minimum of 15 guts were analyzed for each
452 condition. For the SMURF assay ten tubes with 10 flies each were used. For data shown
453 in box plots, the median is given between the first and third quartiles (ends of the box).
454 Whiskers represent the maximum and minimum values of the data. Bar graphs display
455 the mean, with error bars representing the standard deviation.

456 *For the amount of neural tissue and TTCs tissue:* To analyze the effect of the treatment
457 on neural tissue volume and TTCs tissue volume, analysis of covariance (ANCOVA) was
458 performed. The dependent variable was neural tissue volume or TTCs tissue volume, the
459 fixed factor was the treatment, and the covariate was gut volume (Figure 1B, D, E; Figure
460 2D, E; Figure 3A, D, E; Supplementary Figure 1B, C; Supplementary Figure 2).

461 *For other quantifications:* For pairwise comparisons of data sets following a normal
462 distribution (Figure 1C) the unpaired t-test was performed. For pairwise comparisons of
463 data sets not following a normal distribution we used the non-parametric Mann Whitney
464 test (Figure 2A-C; Supplementary Figure 1A).

465

466 **FUNDING**

467 This work was funded by the Spanish Ministerio de Ciencia e Innovación (grant PID2019-
468 107340GB-I00) and Agència de Gestió d'Ajuts Universitaris i de Recerca of the
469 Generalitat de Catalunya (2021SGR00293) to M.M. Work in I.M-A. was funded by an ERC
470 Advanced Grant (ERCAdG 787470 "IntraGutSex"), a UKRI Horizon Europe guarantee grant
471 (EPSRC-ERC EP/Y03298/1), MRC intramural funding and the Francis Crick Institute,
472 which receives its core funding from Cancer Research UK (FC001317 and FC001175), the
473 UK Medical Research Council (FC001317 and FC001175), and the Wellcome Trust
474 (FC001317 and FC001175).

ACKNOWLEDGEMENTS

We thank C. González, M. Milán, C. Estella, J. Morante, B. Hudry, M. Corominas, F. Serras, BDSC and DSHB for reagents and members of the Corominas' and Serras' laboratories for insightful discussions. We are grateful to Q. Zhu and O. Ramirez for their assistance with early pilot experiments that helped shape this research. We are indebted to our colleagues F. Cebrià, M. Milán, M. Corominas, F. Serras, B. Payer and the CCiTUB technological platform for their invaluable support and encouragement during this project.

CONFLICT OF INTERESTS

The authors declare that they have no conflict of interest.

CONTRIBUTIONS

Conceptualization: M.M.; Methodology: M.R-M., M.B., P.G., A.M., S.R., I.M-A., M.M.; Investigation: M.R-M., M.M.; Formal Analysis: M.R-M., P.G., A.M., S.R., I.M-A., M.M.; Validation: M.R-M., M.M.; Visualization: M.R-M., M.M.; Data Curation: M.R-M., M.M.; Resources: P.G., A.M., I.M-A.; Supervision: M.M.; Project Administration: M.M.; Funding Acquisition: M.M.; Writing – Original Draft: M.M. with contributions from all the authors.

REFERENCES

Amcheslavsky, A., Jiang, J., Ip, Y.T., 2009. Tissue Damage-Induced Intestinal Stem Cell Division in Drosophila. Cell Stem Cell 4, 49–61. https://doi.org/10.1016/j.stem.2008.10.016

Ameku, T., Beckwith, H., Blackie, L., Miguel-Aliaga, I., 2020. Food, microbes, sex and old age: on the plasticity of gastrointestinal innervation. Curr. Opin. Neurobiol. 62, 83–91. https://doi.org/10.1016/j.conb.2019.12.004

Antonello, Z.A., Reiff, T., Ballesta-Illan, E., Dominguez, M., 2015. Robust intestinal homeostasis relies on cellular plasticity in enteroblasts mediated by miR-8–Escargot switch. EMBO J. 34, 2025–2041. https://doi.org/10.15252/embj.201591517

Bashaw, G.J., Klein, R., 2010. Signaling from Axon Guidance Receptors. Cold Spring Harb. Perspect. Biol. 2, a001941–a001941. https://doi.org/10.1101/cshperspect.a001941

Bell, L.R., Horabin, J.I., Schedl, P., Cline, T.W., 1991. Positive autoregulation of Sex-lethal by alternative splicing maintains the female determined state in Drosophila. Cell 65, 229–239. https://doi.org/10.1016/0092-8674(91)90157-T

Bell, L.R., Maine, E.M., Schedl, P., Cline, T.W., 1988. Sex-lethal, a Drosophila sex determination switch gene, exhibits sex-specific RNA splicing and sequence similarity to RNA binding proteins. Cell 55, 1037–1046. https://doi.org/10.1016/0092-8674(88)90248-6

Belote, J.M., McKeown, M., Boggs, R.T., Ohkawa, R., Sosnowski, B.A., 1989. Molecular genetics of *transformer* , a genetic switch controlling sexual differentiation in *Drosophila*. Dev. Genet. 10, 143–154. https://doi.org/10.1002/dvg.1020100304

Bentley, D., Toroian-Raymond, A., 1981. Embryonic and postembryonic morphogenesis of a grasshopper interneuron. J. Comp. Neurol. 201, 507–518. https://doi.org/10.1002/cne.902010404

Bernsen, J., 1986. Dynamic Thresholding of Gray Level Image. Proc. Int. Conf. Pattern Recognit. Berl. ICPR 86 1251–1255.

Billuart, P., Winter, C.G., Maresh, A., Zhao, X., Luo, L., 2001. Regulating Axon Branch Stability. Cell 107, 195–207. https://doi.org/10.1016/S0092-8674(01)00522-0

Blackie, L., Gaspar, P., Mosleh, S., Lushchak, O., Kong, L., Jin, Y., Zielinska, A.P., Cao, B., Mineo, A., Silva, B., Ameku, T., Lim, S.E., Mao, Y., Prieto-Godino, L., Schoborg, T., Varela, M., Mahadevan, L., Miguel-Aliaga, I., 2024. The sex of organ geometry. Nature 630, 392–400. https://doi.org/10.1038/s41586-024-07463-4

Boggs, R.T., Gregor, P., Idriss, S., Belote, J.M., McKeown, M., 1987. Regulation of sexual differentiation in D. melanogaster via alternative splicing of RNA from the transformer gene. Cell 50, 739–747. https://doi.org/10.1016/0092-8674(87)90332-1

Bucher, D., Pflüger, H.-J., 2000. Directional sensitivity of an identified wind-sensitive interneuron during the postembryonic development of the locust. J. Insect Physiol. 46, 1545–1556. https://doi.org/10.1016/S0022-1910(00)00078-0

Buchon, N., Osman, D., David, F.P.A., Yu Fang, H., Boquete, J.-P., Deplancke, B., Lemaitre, B., 2013. Morphological and Molecular Characterization of Adult Midgut Compartmentalization in Drosophila. Cell Rep. 3, 1725–1738. https://doi.org/10.1016/j.celrep.2013.04.001

Chen, J., Reiher, W., Hermann-Luibl, C., Sellami, A., Cognigni, P., Kondo, S., Helfrich-Förster, C., Veenstra, J.A., Wegener, C., 2016. Allatostatin A Signalling in Drosophila Regulates Feeding and Sleep and Is Modulated by PDF. PLOS Genet. 12, e1006346. https://doi.org/10.1371/journal.pgen.1006346

Cirillo, C., Brihmat, N., Castel-Lacanal, E., Le Friec, A., Barbieux-Guillot, M., Raposo, N., Pariente, J., Viguier, A., Simonetta-Moreau, M., Albucher, J.-F., Olivot, J.-M., Desmoulin, F., Marque, P., Chollet, F., Loubinoux, I., 2020. Post-stroke remodeling processes in animal models and humans. J. Cereb. Blood Flow Metab. 40, 3–22. https://doi.org/10.1177/0271678X19882788

Cognigni, P., Bailey, A.P., Miguel-Aliaga, I., 2011. Enteric Neurons and Systemic Signals Couple Nutritional and Reproductive Status with Intestinal Homeostasis. Cell Metab. 13, 92–104. https://doi.org/10.1016/j.cmet.2010.12.010

Cui, X., Meiselman, M.R., Thornton, S.N., Yapici, N., 2024. A gut-brain-gut interoceptive circuit loop gates sugar ingestion in Drosophila. https://doi.org/10.1101/2024.09.02.610892

Gao, Z., Pang, Z., Chen, Y., Lei, G., Zhu, S., Li, G., Shen, Y., Xu, W., 2022. Restoring After Central Nervous System Injuries: Neural Mechanisms and Translational

Applications of Motor Recovery. Neurosci. Bull. 38, 1569–1587. https://doi.org/10.1007/s12264-022-00959-x

Hadjieconomou, D., King, G., Gaspar, P., Mineo, A., Blackie, L., Ameku, T., Studd, C., De Mendoza, A., Diao, F., White, B.H., Brown, A.E.X., Plaçais, P.-Y., Préat, T., Miguel-Aliaga, I., 2020. Enteric neurons increase maternal food intake during reproduction. Nature 587, 455–459. https://doi.org/10.1038/s41586-020-2866-8

Hakeda-Suzuki, S., Ng, J., Tzu, J., Dietzl, G., Sun, Y., Harms, M., Nardine, T., Luo, L., Dickson, B.J., 2002. Rac function and regulation during Drosophila development. Nature 416, 438–442. https://doi.org/10.1038/416438a

Hérault, C., Pihl, T., Hudry, B., 2024. Cellular sex throughout the organism underlies somatic sexual differentiation. Nat. Commun. 15, 6925. https://doi.org/10.1038/s41467-024-51228-6

Holsopple, J.M., Cook, K.R., Popodi, E.M., 2022. Enteroendocrine cell expression of split-GAL4 drivers bearing regulatory sequences associated with panneuronally expressed genes in Drosophila melanogaster. Open Access.

Howard, A.M., LaFever, K.S., Fenix, A.M., Scurrah, C.R., Lau, K.S., Burnette, D.T., Bhave, G., Ferrell, N., Page-McCaw, A., 2019. DSS-induced damage to basement membranes is repaired by matrix replacement and crosslinking. J. Cell Sci. 132, jcs226860. https://doi.org/10.1242/jcs.226860

Hudry, B., De Goeij, E., Mineo, A., Gaspar, P., Hadjieconomou, D., Studd, C., Mokochinski, J.B., Kramer, H.B., Plaçais, P.-Y., Preat, T., Miguel-Aliaga, I., 2019. Sex Differences in Intestinal Carbohydrate Metabolism Promote Food Intake and Sperm Maturation. Cell 178, 901-918.e16. https://doi.org/10.1016/j.cell.2019.07.029

Hudry, B., Khadayate, S., Miguel-Aliaga, I., 2016. The sexual identity of adult intestinal stem cells controls organ size and plasticity. Nature 530, 344–348. https://doi.org/10.1038/nature16953

Hyer, M.M., Phillips, L.L., Neigh, G.N., 2018. Sex Differences in Synaptic Plasticity: Hormones and Beyond. Front. Mol. Neurosci. 11, 266. https://doi.org/10.3389/fnmol.2018.00266

Inoue, K., Hoshijima, K., Sakamoto, H., Shimura, Y., 1990. Binding of the Drosophila Sex-lethal gene product to the alternative splice site of transformer primary transcript. Nature 344, 461–463. https://doi.org/10.1038/344461a0

Jenett, A., Rubin, G.M., Ngo, T.-T.B., Shepherd, D., Murphy, C., Dionne, H., Pfeiffer, B.D., Cavallaro, A., Hall, D., Jeter, J., Iyer, N., Fetter, D., Hausenfluck, J.H., Peng, H., Trautman, E.T., Svirskas, R.R., Myers, E.W., Iwinski, Z.R., Aso, Y., DePasquale, G.M., Enos, A., Hulamm, P., Lam, S.C.B., Li, H.-H., Laverty, T.R., Long, F., Qu, L., Murphy, S.D., Rokicki, K., Safford, T., Shaw, K., Simpson, J.H., Sowell, A., Tae, S., Yu, Y., Zugates, C.T., 2012. A GAL4-Driver Line Resource for Drosophila Neurobiology. Cell Rep. 2, 991–1001. https://doi.org/10.1016/j.celrep.2012.09.011

Jiang, H., Tian, A., Jiang, J., 2016. Intestinal stem cell response to injury: lessons from Drosophila. Cell. Mol. Life Sci. 73, 3337–3349. https://doi.org/10.1007/s00018-016-2235-9

Kania, A., Klein, R., 2016. Mechanisms of ephrin–Eph signalling in development, physiology and disease. Nat. Rev. Mol. Cell Biol. 17, 240–256. https://doi.org/10.1038/nrm.2015.16

Kapur, J.N., Sahoo, P.K., Wong, A.K.C., 1985. A new method for gray-level picture thresholding using the entropy of the histogram. Comput. Vis. Graph. Image Process. 29, 273–285. https://doi.org/10.1016/0734-189X(85)90125-2

Kenmoku, H., Ishikawa, H., Ote, M., Kuraishi, T., Kurata, S., 2016. A subset of neurons controls the permeability of the peritrophic matrix and midgut structure in *Drosophila* adults. J. Exp. Biol. jeb.122960. https://doi.org/10.1242/jeb.122960

Kirby, E.D., Andrushko, J.W., Rinat, S., D'Arcy, R.C.N., Boyd, L.A., 2024. Investigating female versus male differences in white matter neuroplasticity associated with complex visuo-motor learning. Sci. Rep. 14, 5951. https://doi.org/10.1038/s41598-024-56453-z

Ksiazek-Winiarek, D.J., Szpakowski, P., Glabinski, A., 2015. Neural Plasticity in Multiple Sclerosis: The Functional and Molecular Background. Neural Plast. 2015, 1–11. https://doi.org/10.1155/2015/307175

Kuraishi, T., Kenmoku, H., Kurata, S., 2015. From mouth to anus: Functional and structural relevance of enteric neurons in the Drosophila melanogaster gut. Insect Biochem. Mol. Biol. 67, 21–26. https://doi.org/10.1016/j.ibmb.2015.07.003

Lee, S., Stevens, C.F., 2007. General design principle for scalable neural circuits in a vertebrate retina. Proc. Natl. Acad. Sci. 104, 12931–12935. https://doi.org/10.1073/pnas.0705469104

Lemaitre, B., Miguel-Aliaga, I., 2013. The Digestive Tract of *Drosophila melanogaster*. Annu. Rev. Genet. 47, 377–404. https://doi.org/10.1146/annurev-genet-111212-133343

Li, C.H., Lee, C.K., 1993. Minimum cross entropy thresholding. Pattern Recognit. 26, 617–625. https://doi.org/10.1016/0031-3203(93)90115-D

Linneweber, G.A., Jacobson, J., Busch, K.E., Hudry, B., Christov, C.P., Dormann, D., Yuan, M., Otani, T., Knust, E., de Bono, M., Miguel-Aliaga, I., 2014. Neuronal Control of Metabolism through Nutrient-Dependent Modulation of Tracheal Branching. Cell 156, 69–83. https://doi.org/10.1016/j.cell.2013.12.008

Lund-Ricard, Y., Cormier, P., Morales, J., Boutet, A., 2020. mTOR Signaling at the Crossroad between Metazoan Regeneration and Human Diseases. Int. J. Mol. Sci. 21, 2718. https://doi.org/10.3390/ijms21082718

Luo, L., O'Leary, D.D.M., 2005. AXON RETRACTION AND DEGENERATION IN DEVELOPMENT AND DISEASE. Annu. Rev. Neurosci. 28, 127–156. https://doi.org/10.1146/annurev.neuro.28.061604.135632

Mahar, M., Cavalli, V., 2018. Intrinsic mechanisms of neuronal axon regeneration. Nat. Rev. Neurosci. 19, 323–337. https://doi.org/10.1038/s41583-018-0001-8

Mank, J.E., Rideout, E.J., 2021. Developmental mechanisms of sex differences: from cells to organisms. Development 148. https://doi.org/10.1242/dev.199750

Marianes, A., Spradling, A.C., 2013. Physiological and stem cell compartmentalization within the Drosophila midgut. eLife 2, e00886. https://doi.org/10.7554/eLife.00886

McGuire, S.E., Le, P.T., Osborn, A.J., Matsumoto, K., Davis, R.L., 2003. Spatiotemporal Rescue of Memory Dysfunction in *Drosophila*. Science 302, 1765–1768. https://doi.org/10.1126/science.1089035

Menon, K.P., Carrillo, R.A., Zinn, K., 2013. Development and plasticity of the *Drosophila* larval neuromuscular junction. WIREs Dev. Biol. 2, 647–670. https://doi.org/10.1002/wdev.108

Miguel-Aliaga, I., Jasper, H., Lemaitre, B., 2018. Anatomy and Physiology of the Digestive Tract of *Drosophila melanogaster*. Genetics 210, 357–396. https://doi.org/10.1534/genetics.118.300224

Min, S., Oh, Y., Verma, P., Whitehead, S.C., Yapici, N., Van Vactor, D., Suh, G.S., Liberles, S., 2021. Control of feeding by Piezo-mediated gut mechanosensation in Drosophila. eLife 10, e63049. https://doi.org/10.7554/eLife.63049

Murphy, T.H., Corbett, D., 2009. Plasticity during stroke recovery: from synapse to behaviour. Nat. Rev. Neurosci. 10, 861–872. https://doi.org/10.1038/nrn2735

Nudo, R.J., 2003. Functional and structural plasticity in motor cortex: implications for stroke recovery. Phys. Med. Rehabil. Clin. N. Am. 14, S57–S76. https://doi.org/10.1016/S1047-9651(02)00054-2

Olds, W.H., Xu, T., 2014. Regulation of food intake by mechanosensory ion channels in enteric neurons. eLife 3, e04402. https://doi.org/10.7554/eLife.04402

Ollion, J., Cochennec, J., Loll, F., Escudé, C., Boudier, T., 2013. TANGO: a generic tool for high-throughput 3D image analysis for studying nuclear organization. Bioinformatics 29, 1840–1841. https://doi.org/10.1093/bioinformatics/btt276

Oswald, M.C.W., Garnham, N., Sweeney, S.T., Landgraf, M., 2018. Regulation of neuronal development and function by ROS. FEBS Lett. 592, 679–691. https://doi.org/10.1002/1873-3468.12972

Pasterkamp, R.J., 2012. Getting neural circuits into shape with semaphorins. Nat. Rev. Neurosci. 13, 605–618. https://doi.org/10.1038/nrn3302

Perochon, J., Yu, Y., Aughey, G.N., Medina, A.B., Southall, T.D., Cordero, J.B., 2021. Dynamic adult tracheal plasticity drives stem cell adaptation to changes in intestinal homeostasis in Drosophila. Nat. Cell Biol. 23, 485–496. https://doi.org/10.1038/s41556-021-00676-z

Petersen, E.D., Sharkey, E.D., Pal, A., Shafau, L.O., Zenchak-Petersen, J., Peña, A.J., Aggarwal, A., Prakash, M., Hochgeschwender, U., 2022. Restoring Function After Severe Spinal Cord Injury Through BioLuminescent-OptoGenetics. Front. Neurol. 12, 792643. https://doi.org/10.3389/fneur.2021.792643

Petsakou, A., Liu, Yifang, Liu, Ying, Comjean, A., Hu, Y., Perrimon, N., 2023. Cholinergic neurons trigger epithelial Ca2+ currents to heal the gut. Nature 623, 122–131. https://doi.org/10.1038/s41586-023-06627-y

Prosperini, L., Piattella, M.C., Giannì, C., Pantano, P., 2015. Functional and Structural Brain Plasticity Enhanced by Motor and Cognitive Rehabilitation in Multiple Sclerosis. Neural Plast. 2015, 1–12. https://doi.org/10.1155/2015/481574

Regan, J.C., Khericha, M., Dobson, A.J., Bolukbasi, E., Rattanavirotkul, N., Partridge, L., 2016. Sex difference in pathology of the ageing gut mediates the greater response of female lifespan to dietary restriction. eLife 5. https://doi.org/10.7554/elife.10956

Regan, J.C., Lu, Y.-X., Ureña, E., Meilenbrock, R.L., Catterson, J.H., Kißler, D., Fröhlich, J., Funk, E., Partridge, L., 2022. Sexual identity of enterocytes regulates autophagy to determine intestinal health, lifespan and responses to rapamycin. Nat. Aging 2, 1145–1158. https://doi.org/10.1038/s43587-022-00308-7

Reiff, T., Jacobson, J., Cognigni, P., Antonello, Z., Ballesta, E., Tan, K.J., Yew, J.Y., Dominguez, M., Miguel-Aliaga, I., 2015. Endocrine remodelling of the adult intestine sustains reproduction in Drosophila. eLife 4. https://doi.org/10.7554/elife.06930

Rera, M., Clark, R.I., Walker, D.W., 2012. Intestinal barrier dysfunction links metabolic and inflammatory markers of aging to death in Drosophila. Proc. Natl. Acad. Sci. U. S. A. 109, 21528–21533. https://doi.org/10.1073/pnas.1215849110

Rodríguez, A., Foronda, D., Córdoba, S., Felipe-Cordero, D., Baonza, A., Miguez, D.G., Estella, C., 2024. Cell proliferation and Notch signaling coordinate the formation of epithelial folds in the *Drosophila* leg. Development 151, dev202384. https://doi.org/10.1242/dev.202384

Sampaio-Baptista, C., Sanders, Z.-B., Johansen-Berg, H., 2018. Structural Plasticity in Adulthood with Motor Learning and Stroke Rehabilitation. Annu. Rev. Neurosci. 41, 25–40. https://doi.org/10.1146/annurev-neuro-080317-062015

Sanal, N., Keding, L., Gigengack, U., Michalke, E., Rumpf, S., 2023. TORC1 regulation of dendrite regrowth after pruning is linked to actin and exocytosis. PLOS Genet. 19, e1010526. https://doi.org/10.1371/journal.pgen.1010526

Sato, Y., Nakajima, S., Shiraga, N., Atsumi, H., Yoshida, S., Koller, T., Gerig, G., Kikinis, R., 1998. Three-dimensional multi-scale line filter for segmentation and visualization of curvilinear structures in medical images. Med. Image Anal. 2, 143–168. https://doi.org/10.1016/S1361-8415(98)80009-1

Schindelin, J., Arganda-Carreras, I., Frise, E., Kaynig, V., Longair, M., Pietzsch, T., Preibisch, S., Rueden, C., Saalfeld, S., Schmid, B., Tinevez, J.-Y., White, D.J., Hartenstein, V., Eliceiri, K., Tomancak, P., Cardona, A., 2012. Fiji: an open-source platform for biological-image analysis. Nat. Methods 9, 676–682. https://doi.org/10.1038/nmeth.2019

Sosnowski, B.A., Belote, J.M., McKeown, M., 1989. Sex-specific alternative splicing of RNA from the transformer gene results from sequence-dependent splice site blockage. Cell 58, 449–459. https://doi.org/10.1016/0092-8674(89)90426-1

Tamamouna, V., Rahman, M.M., Petersson, M., Charalambous, I., Kux, K., Mainor, H., Bolender, V., Isbilir, B., Edgar, B.A., Pitsouli, C., 2021. Remodelling of oxygen-transporting tracheoles drives intestinal regeneration and tumorigenesis in Drosophila. Nat. Cell Biol. 23, 497–510. https://doi.org/10.1038/s41556-021-00674-1

Tedeschi, A., Bradke, F., 2017. Spatial and temporal arrangement of neuronal intrinsic and extrinsic mechanisms controlling axon regeneration. Curr. Opin. Neurobiol. 42, 118–127. https://doi.org/10.1016/j.conb.2016.12.005

Tian, A., Morejon, V., Kohoutek, S., Huang, Y., Deng, W., Jiang, J., 2022. Damage-induced regeneration of the intestinal stem cell pool through enteroblast mitosis in the *Drosophila* midgut. EMBO J. 41, e110834. https://doi.org/10.15252/embj.2022110834

Titos, I., Juginović, A., Vaccaro, A., Nambara, K., Gorelik, P., Mazor, O., Rogulja, D., 2023. A gut-secreted peptide suppresses arousability from sleep. Cell 186, 1382-1397.e21. https://doi.org/10.1016/j.cell.2023.02.022

Turtzo, L.C., McCullough, L.D., 2008. Sex Differences in Stroke. Cerebrovasc. Dis. 26, 462–474. https://doi.org/10.1159/000155983

Watts, R.J., Hoopfer, E.D., Luo, L., 2003. Axon Pruning during Drosophila Metamorphosis. Neuron 38, 871–885. https://doi.org/10.1016/S0896-6273(03)00295-2

Weaver, L.N., Ma, T., Drummond-Barbosa, D., 2020. Analysis of Gal4 Expression Patterns in Adult *Drosophila* Females. G3 GenesGenomesGenetics 10, 4147–4158. https://doi.org/10.1534/g3.120.401676

Williams, D.W., Kondo, S., Krzyzanowska, A., Hiromi, Y., Truman, J.W., 2006. Local caspase activity directs engulfment of dendrites during pruning. Nat. Neurosci. 9, 1234–1236. https://doi.org/10.1038/nn1774

Williams, D.W., Truman, J.W., 2005. Cellular mechanisms of dendrite pruning in *Drosophila* : insights from in vivo time-lapse of remodeling dendritic arborizing sensory neurons. Development 132, 3631–3642. https://doi.org/10.1242/dev.01928

Wu, S.-C., Liao, C.-W., Pan, R.-L., Juang, J.-L., 2012. Infection-Induced Intestinal Oxidative Stress Triggers Organ-to-Organ Immunological Communication in Drosophila. Cell Host Microbe 11, 410–417. https://doi.org/10.1016/j.chom.2012.03.004

Yang, C., Merlin, D., 2024. Unveiling Colitis: A Journey through the Dextran Sodium Sulfate-induced Model. Inflamm. Bowel Dis. 30, 844–853. https://doi.org/10.1093/ibd/izad312

Yaniv, S.P., Schuldiner, O., 2016. A fly's view of neuronal remodeling. WIREs Dev. Biol. 5, 618–635. https://doi.org/10.1002/wdev.241

Yoshida, S., Hong, S., Suzuki, T., Nada, S., Mannan, A.M., Wang, J., Okada, M., Guan, K.-L., Inoki, K., 2011. Redox Regulates Mammalian Target of Rapamycin Complex 1 (mTORC1) Activity by Modulating the TSC1/TSC2-Rheb GTPase Pathway. J. Biol. Chem. 286, 32651–32660. https://doi.org/10.1074/jbc.M111.238014

Yu, C., An, Z., Zhao, W., Wang, W., Gao, C., Liu, S., Wang, J., Wu, J., 2015. Sex Differences in Stroke Subtypes, Severity, Risk Factors, and Outcomes among Elderly Patients with Acute Ischemic Stroke. Front. Aging Neurosci. 7. https://doi.org/10.3389/fnagi.2015.00174

Zhang, Y., Park, J., Han, S.-J., Yang, S.Y., Yoon, H.J., Park, I., Woo, H.A., Lee, S.-R., 2020. Redox regulation of tumor suppressor PTEN in cell signaling. Redox Biol. 34, 101553. https://doi.org/10.1016/j.redox.2020.101553